Development 136, 3515-3524 (2009) doi:10.1242/dev.037507

Patched 1 is a crucial determinant of asymmetry and digit number in the vertebrate limb

Natalie C. Butterfield[1], Vicki Metzis[1], Edwina McGlinn[2], Stephen J. Bruce[1], Brandon J. Wainwright[1] and Carol Wicking[1,*]

The vertebrate hedgehog receptor patched 1 (Ptc1) is crucial for negative regulation of the sonic hedgehog (Shh) pathway during anterior-posterior patterning of the limb. We have conditionally inactivated *Ptc1* in the mesenchyme of the mouse limb using *Prx1*-Cre. This results in constitutive activation of hedgehog (Hh) signalling during the early stages of limb budding. Our data suggest that variations in the timing and efficiency of Cre-mediated excision result in differential forelimb and hindlimb phenotypes. Hindlimbs display polydactyly (gain of digits) and a molecular profile similar to the *Gli3* mutant *extra-toes*. Strikingly, forelimbs are predominantly oligodactylous (displaying a loss of digits), with a symmetrical, mirror-image molecular profile that is consistent with re-specification of the anterior forelimb to a posterior identity. Our data suggest that this is related to very early inactivation of *Ptc1* in the forelimb perturbing the gene regulatory networks responsible for both the pre-patterning and the subsequent patterning stages of limb development. These results establish the importance of the downstream consequences of Hh pathway repression, and identify Ptc1 as a key player in limb patterning even prior to the onset of Shh expression.

KEY WORDS: Patched 1, Sonic hedgehog signalling, Limb development, *Prx1*-Cre, Shh/Grem1/FGF loop, Mouse

INTRODUCTION

Hedgehog (Hh) signalling is essential for the correct patterning of virtually every vertebrate organ system, including the limb (Hill, 2007; Ingham and McMahon, 2001). In the absence of a hedgehog ligand (Sonic, Shh; Indian or Desert), the transmembrane receptor patched 1 (Ptc1; also known as Ptch1) constitutively inhibits the transducer of the Hh signal, smoothened (Smo) (Chen and Struhl, 1996; Marigo et al., 1996a). In this repressed state, proteolytically cleaved Gli transcription factors, primarily Gli3, translocate to the nucleus to repress target genes. Upon binding of a hedgehog ligand to Ptc1, inhibition of Smo is relieved, Gli cleavage is inhibited, and full-length Gli proteins are converted to transcriptional activators. Importantly Ptc1, an inhibitor of the pathway, is transcriptionally upregulated in response to Hh signalling, creating a negative-feedback loop that is crucial for tight spatiotemporal control of signalling levels. Disruption of this feedback loop by inactivation of *Ptc1* in mice results in inappropriate ligand-independent activation of the Hh pathway, and early embryonic lethality around 9.5 days post coitum (dpc) (Ellis et al., 2003; Goodrich et al., 1997).

In the limb, Shh is secreted from a group of posterior mesenchymal cells called the zone of polarizing activity (ZPA) (Riddle et al., 1993). The posteriorly biased Shh gradient, together with a temporal gradient of exposure to the Shh signal, specifies digit number and identity (reviewed by McGlinn and Tabin, 2006). Shh successively inhibits the cleavage of full-length Gli3 (Gli3FL) to the repressor form (Gli3R) from posterior to anterior (Wang et al., 2000), and this interplay between Shh and Gli3 is crucial in defining anterior-posterior (AP) limb patterning (Litingtung et al., 2002; te Welscher et al., 2002b). The *Shh* null mouse hindlimb has a single digit corresponding to the most anterior digit 1 (Chiang et al., 2001), whereas the *extra-toes* (*Gli3*$^{Xt/Xt}$) mouse mutant lacks functional Gli3 and displays extra digits, or polydactyly (Hui and Joyner, 1993). While Gli3R is regarded as the primary effector of AP patterning in the limb, the role of Gli3FL in this process is the subject of some debate (Hill et al., 2009; Wang et al., 2007a; Wang et al., 2007b).

The nascent limb bud is subject to an exquisitely controlled network of gene regulatory loops that pattern the limb bud both before and after expression of *Shh*. Soon after emergence of the limb bud, an AP pre-pattern is established whereby anterior Gli3R restricts *Hand2* expression to the posterior, and Hand2 reciprocally limits *Gli3* to the anterior (te Welscher et al., 2002a). At this stage, the posterior restriction of 5′Hoxd genes (those genes at the 5′ end of the Hoxd cluster) is crucial to final AP limb asymmetry, as these genes subsequently trigger expression of *Shh* specifically in the posterior limb (Tarchini et al., 2006; Zakany et al., 2004). Around the same time, Bmp4 induces expression of the BMP antagonist gremlin (*Grem1*), thus initiating the first of a number of finely tuned regulatory loops linking Shh signalling in the ZPA with FGF signalling from the distal apical ectodermal ridge (AER) (Benazet et al., 2009). Downregulation of *Bmp4* by Grem1 enables Shh signalling from the ZPA, thus establishing the Shh/Grem1/FGF loop, whereby Shh induces *Grem1* expression in the mesenchyme. This then allows FGF signalling from the AER, which in turn maintains *Shh* in the ZPA (Khokha et al., 2003; Zuniga et al., 1999). A recent study suggests that limb outgrowth ceases when the Shh/Grem1/FGF loop drives FGF signalling to high enough levels to inhibit *Grem1* expression (Verheyden and Sun, 2008). However, previous studies in the chick indicate that the inability of *Shh* expressing cells and their descendants to express *Grem1* contributes to termination of limb outgrowth, as *Grem1*-expressing cells move beyond the influence of Shh from the ZPA (Nissim et al., 2006; Scherz et al., 2004).

Ptc1 null mice, or mice in which *Ptc1* is ubiquitously inactivated, die prior to the initiation of limb budding (Ellis et al., 2003; Goodrich et al., 1997). Despite elegant studies involving transgenic rescue of

[1]The University of Queensland, Institute for Molecular Bioscience, Queensland 4072, Australia. [2]Harvard Medical School, 77 Avenue Louis Pasteur, Boston, MA 02115, USA.

*Author for correspondence (c.wicking@imb.uq.edu.au)

Accepted 21 August 2009

Ptc1 null mice (Milenkovic et al., 1999), the effects of *Ptc1* inactivation in the early limb have not previously been investigated. We have used Cre recombinase driven by a *Prx1* enhancer (Logan et al., 2002) to conditionally remove functional *Ptc1* from the limb mesenchyme. This results in high-level ligand-independent activation of the Hh pathway across the entire limb. *Ptc1* inactivation occurs before and after establishment of the ZPA in the forelimb and hindlimb, respectively, and these variations in timing and the subsequent level of Hh pathway activation are thought to underlie the dramatically altered phenotype produced in each limb. Later and lower levels of signalling in the hindlimb lead to polydactyly (gain of digits), while early and high-level pathway activation in the forelimb predominantly and unexpectedly results in oligodactyly (loss of digits). These forelimbs display a molecular expression profile that is largely symmetrical about the midline of the AP axis, reflecting re-specification of the anterior limb to a posterior fate. In addition, activation of the Hh pathway in a pattern that mirrors *Prx1*-Cre activity suggests that, unlike previous assumptions based on in situ hybridisation analysis of *Ptc1*, most embryonic mesenchyme is competent to activate Hh signalling if stimulated. This highlights the crucial nature of Ptc1-mediated repression.

MATERIALS AND METHODS

Mouse breeding

All animal experimentation was approved by a University of Queensland Animal Ethics Committee and conformed to relevant ethical guidelines. *Prx1-Cre* homozygous male mice (Logan et al., 2002) were mated with females homozygous for the *Ptc1* conditional allele (*Ptc1*$^{c/c}$) (Ellis et al., 2003), on a C57/Bl6/SV129 background. Male offspring heterozygous for both alleles were then backcrossed to *Ptc1*$^{c/c}$ females. The offspring of these crosses were designated wild type (WT; no *Prx1*-Cre and one or two *Ptc1* conditional alleles), heterozygous (*Prx1-Cre:Ptc1*$^{c/wt}$) or homozygous (*Prx1-Cre:Ptc1*$^{c/c}$). For analysis of *Prx1*-Cre activity, females heterozygous for the *Z/AP* reporter transgene were mated to *Prx1-Cre:Ptc1*$^{c/wt}$ males, and offspring were assayed for alkaline phosphatase expression as previously described (Lobe et al., 1999). PCR genotyping for the *Ptc1* conditional transgene was performed as previously described (Ellis et al., 2003). Cre recombinase was detected using the primers: F, 5′-GATATCTCACGTACTGACGGTG-3′; R, 5′-CTGTTT-CACTATCCAGGTTAC-3′.

RNA in situ hybridisation

Whole-mount in situ hybridisation was performed as previously described (Fowles et al., 2003). Probes were: *Shh* [nucleotides 36-678 of the vertebrate hedgehog sequence NM_017221 described by Roelink et al. (Roelink et al., 1994)], *Ptc1* (Hahn et al., 1996), *Gli1*, *Gli3* (C. C. Hui, The Hospital for Sick Children, University of Toronto, Canada), *Hand2* (E. Olson, UT Southwestern Medical Center, Dallas, TX, USA), *Fgf4*, *Fgf8* (G. Martin, University of California San Francisco, CA, USA), *Mkp3*, *Spry1*, *Spry4* (M. Little, The University of Queensland, Australia), *Grem1* (R. Harland, University of California, Berkeley, CA, USA), *Hoxd11* (C. Tabin, Harvard Medical School, Boston, MA, USA), *Hoxd12, Hoxd13* (D. Duboule, University of Geneva, Switzerland), *Msx1* (R. Maas, Brigham and Women's Hospital, Boston, MA, USA), *Msx2* (R. Maxson, University of Southern California, Los Angeles, CA, USA), *Zfp503* (McGlinn et al., 2008), *Pax9*, *Jag1* (McGlinn et al., 2005), and *Bmp2* and *Bmp4* (E. Robertson, University of Oxford, UK).

Reverse transcriptase (RT)-PCR for exon 3 of *Ptc1*

Individual limb pairs (9.5-11.5 dpc) were dissected and epithelium removed with 1 unit/ml dispase (Sigma), 10% foetal calf serum (Biowhittaker) in Puck's Saline A for 1 hour at 37°C. Total RNA was extracted using an RNeasy miniprep kit (QIAGEN). cDNA was reverse transcribed from 1 μg of RNA with pd(N_6) random hexamers and MMLV-RT (Invitrogen) according to the manufacturer's instructions. To ascertain recombination, a region including the exon flanked by *loxP* sites in the *Ptc1* conditional allele (exon 3) was amplified using the primers Exon 2-F (5′-TGGTTGTG-GGTCTCCTCATATT-3′) and Exon 6-R (5′-CACCGTAAAGGAGCG-TTACCTA-3′) to produce 450-bp (WT allele) and 250-bp (deleted allele) products. Actin-positive control products (650 bp) were generated as described by Chen et al. (Chen et al., 2002).

Quantitative real-time PCR

Quantitative real-time PCR on cDNA was performed as previously reported (Bruce et al., 2007), and expression levels normalised against mouse hypoxanthine phosphoribosyltransferase (HPRT) as determined from the ratio of ΔCT values. Primers used were: HPRT (Bruce et al., 2007); Ptc1-F, 5′-GTTCTGGACGGTGCTGTGTC-3′; Ptc1-R, 5′-GCCAGGACGGC-AAAGAAG-3′; Gli1-F, 5′-TCAAGGCCCAATACATGCTG-3′; Gli1-R, 5′-AGGACTTCCGACAGCCTTCA-3′; Ptc2-F, 5′-TGGTAATCCT-CGTGGCCTCT-3′; and Ptc2-R, 5′-GCTACCATGGCTGGTCAGG-3′. Mean of relative expression ± s.d. was determined from biological replicates (n=2-4 samples of two limbs each). Statistical significance was determined using a Student's t-test (*P<0.05, **P<0.01). All amplicons were gel-purified and sequenced to ensure correct product amplification.

BrdU and TUNEL analysis

Proliferating cells were detected by injecting pregnant mice with 10 μl/g bromodeoxyuridine labelling reagent (BrdU; Zymed). Two hours after injection, embryos were dissected, fixed, processed for paraffin wax embedding and sectioned at 8 μM according to standard protocols. BrdU was detected using a biotinylated α-BrdU antibody (Zymed), Vectastain Elite ABC and DAB peroxidase substrate kits (Vector Laboratories), according to the manufacturer's instructions, prior to counterstaining with Nuclear Fast Red (Vector Laboratories). The relative areas occupied by proliferating and non-proliferating cells were quantified using ImageJ software. Mean of relative percentage ± s.e.m. was determined from biological duplicates (>15 technical replicates of <5% variation). Statistical significance was determined using a Student's t-test (***P=0.001). Apoptotic cells in 8 μM limb sections were detected using a Fluorescein In Situ Cell Death Detection Kit (Roche).

Detection of Gli3 protein by western blot

Pooled anterior and posterior 11.5 dpc autopod halves were lysed in RIPA buffer plus complete protease inhibitor cocktail (Roche). Samples in 1×Laemmli sample buffer with 10% β-mercaptoethanol were boiled for 5 minutes prior to electrophoresis through an 8% Tris-glycine gel and transfer onto a PDVF membrane (Millipore) overnight at 30 V. Gli3 protein was detected using a rabbit α-Gli3 antibody (Wang et al., 2000), and α-tubulin by a mouse DMIA antibody (Sigma), with HRP-conjugated secondary antibodies (Zymed) and ECL detection reagents (Amersham).

RESULTS

Inactivation of *Ptc1* upregulates Hh signalling and produces variable gain/loss of digits

The *Prx1-Cre* transgene drives Cre recombinase activity in the early limb mesenchyme (Logan et al., 2002). *Prx1-Cre* heterozygotes were mated with mice homozygous for a conditional allele of *Ptc1* engineered by flanking exon 3 with *loxP* sites (Ellis et al., 2003). Heterozygous *Prx1-Cre:Ptc1*$^{c/wt}$ mice survive to adulthood and are fertile and viable. Homozygous *Prx1-Cre:Ptc1*$^{c/c}$ embryos survive until 14.0 dpc, allowing analysis of the effects of *Ptc1* inactivation in the limb mesenchyme during early limb development. Oedema visible from 13.5 dpc (Fig. 1B,C, arrowheads), and vascular haemorrhage evident at 14.0 dpc (Fig. 1C, arrowheads), are likely to be responsible for the lethality at this stage, although this phenotype has yet to be analysed in detail. Loss of tissue integrity in the distal limb often results in blister formation, which is particularly evident in the interdigital region at 13.5 dpc (arrowhead, Fig. 1H). At these later stages we have also detected defects in chondrogenesis, and characterisation of this phenotype will be presented elsewhere.

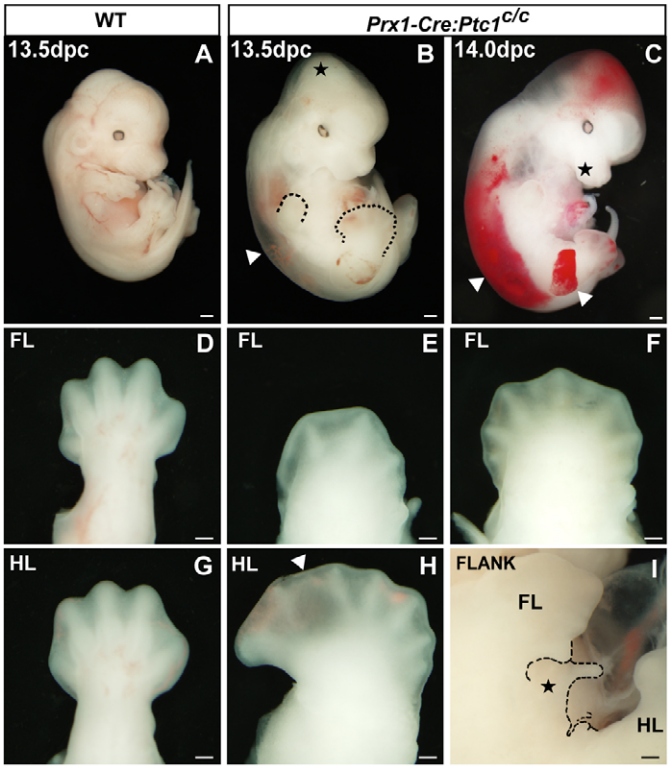

Fig. 1. *Prx1-Cre:Ptc1*$^{c/c}$ embryos display variable polydactyly/oligodactyly, and do not survive past 14.0 dpc. Wild-type (**A**,**D**,**G**) and *Prx1-Cre:Ptc1*$^{c/c}$ (**B**,**C**,**E**,**F**,**H**,**I**) embryos at 13.5 and 14.0 dpc. At 13.5-14.0 dpc, *Prx1-Cre:Ptc1*$^{c/c}$ embryos display overgrowth of the cranial mesenchyme, the inter-limb flank region and the maxilla (stars, B,C,I). By 14.0 dpc, embryos display blistering (also in the distal limb at 13.5 dpc, arrowhead, H), and vascular haemorrhage into oedemic areas (arrowheads, C; oedema also visible at 13.5 dpc, arrowhead, B). The majority (76%) of 13.5 dpc *Prx1-Cre:Ptc1*$^{c/c}$ forelimbs are oligodactylous (E), while 24% are polydactylous (F). All *Prx1-Cre:Ptc1*$^{c/c}$ hindlimbs display asymmetrical polydactyly (H). Scale bars: 500 μM in A-C; 200 μM in D-I.

Prx1-Cre:Ptc1$^{c/c}$ hindlimbs display polydactyly (Fig. 1H) with expansion of anterior tissue reminiscent of the *Gli3*$^{Xt/Xt}$ limb and other Hh gain-of-function mouse models (Hill et al., 2003). Unexpectedly, the forelimb primarily displays an opposing phenotype, with 76% of 13.5 dpc *Prx1-Cre:Ptc1*$^{c/c}$ forelimbs analysed showing evidence of fewer digit primordia (oligodactyly; Fig. 1E; n=41). A minority (24%) of 13.5 dpc *Prx1-Cre:Ptc1*$^{c/c}$ forelimbs are polydactylous (Fig. 1F), but most retain the symmetry of shape of the oligodactylous forelimb, rather than the anterior expansion observed in the hindlimb (Fig. 1; compare F to H). Mesenchymal overgrowth visible in the dorsal cranium, maxilla and flank (star, Fig. 1B,C,I) correlates with additional sites of *Prx1*-Cre activity (see below).

We sought to define the spatiotemporal boundaries of *Prx1*-Cre activity relative to both *Ptc1* excision and subsequent activation of the Hh pathway in the *Prx1-Cre:Ptc1*$^{c/c}$ limbs. Deletion of exon 3 of *Ptc1* results in the upregulation of a transcript that encodes a non-functional protein incapable of dampening pathway activity via negative autoregulation. However, similar to wild-type *Ptc1* and *Gli1* transcripts (Goodrich et al., 1996; Marigo et al., 1996b), this truncated transcript acts as a robust marker of pathway activation. Using a probe capable of detecting both wild-type and exon 3-deleted *Ptc1*, whole-mount in situ hybridisation revealed wild-type *Ptc1* expression primarily in a restricted domain in the limb bud and in the vibrissae at 12.5 dpc (Fig. 2A). Upon *Ptc1* inactivation, expression was visible throughout the limb mesenchyme (Fig. 2B), and across the embryo in a pattern correlating closely with sites of *Prx1*-Cre activity (Fig. 2, compare B with D), as visualised by alkaline phosphatase expression in the Z/AP reporter assay (Lobe et al., 1999). In addition to the limb, these sites include the mesenchyme of the flank, the distal maxilla and the dorsal cranium, although expression of *Ptc1* appears to be less robust in this latter region (Fig. 2B,D; Fig. S1B,E in the supplementary material) (see also Logan et al., 2002). The extent of Hh pathway activation revealed by *Ptc1* was confirmed by *Gli1* expression (Fig. 2C). A probe directed specifically to the deleted exon 3 of *Ptc1* showed no hybridisation to regions of the embryo expressing *Prx1*-Cre outside the normal domains of *Ptc1* expression (data not shown), confirming that the ectopic *Ptc1* transcript is the non-functional deleted form.

The precise timing of *Ptc1* inactivation was determined by RT-PCR of a region spanning exon 3. Detection of only the exon 3-deleted *Ptc1* allele in three out of four 9.5 dpc *Prx1-Cre:Ptc1*$^{c/c}$ forelimb samples indicates, within the limits of detection by RT-PCR, complete excision of exon 3 before 9.5 dpc (Fig. 2E). Wild-type *Ptc1* was still detectable in the *Prx1-Cre:Ptc1*$^{c/c}$ hindlimb at 10.5 dpc, but not at 11.5 dpc, indicating that exon 3 deletion approaches completion in the hindlimb between 10.5 dpc and 11.5 dpc (Fig. 2F). The relationship between *Ptc1* exon 3 excision and Hh pathway activation was assessed by quantitative real-time PCR for *Ptc1* and *Gli1* transcripts. These data confirm that earlier excision in the forelimb (Fig. 2E,F) results in earlier and higher upregulation of *Ptc1* and *Gli1* in the forelimb compared with in the hindlimb (Fig. 2G,H). This provides a likely cause for the phenotypic differences observed between these limbs. A similar trend in expression of a second pathway inhibitor, patched 2 (*Ptc2*; also known as *Ptch2*), was also observed (Fig. 2I), although upregulation in both *Prx1-Cre:Ptc1*$^{c/c}$ forelimbs and hindlimbs did not reach significance until 11.5 dpc. Because we observed no obvious attenuation of Hh signalling at the stages analysed, it is unlikely that upregulated *Ptc2* is acting redundantly to significantly dampen pathway activity in this context. Taken together, these data confirm that excision of *Ptc1* and subsequent upregulation of the Hh pathway correlate closely with sites of *Prx1*-Cre expression, and demonstrate a delay in these events in the hindlimb compared with in the forelimb.

The Gli3 protein gradient is disrupted in *Prx1-Cre:Ptc1*$^{c/c}$ limbs

Based on the negative regulation of both *Gli3* transcript and Gli3R production by Shh signalling (Marigo et al., 1996b; Wang et al., 2000), constitutive Hh pathway activation should result in decreased levels of Gli3R. Anterior and posterior halves of 11.5 dpc limbs were assayed for Gli3FL (190 kDa) and Gli3R (83 kDa) by western blot. In control limbs, the anteroposterior gradient of Gli3R (Fig. 2J) was consistent with published results (Chen et al., 2004; Litingtung et al., 2002; Wang et al., 2000). By contrast, this Gli3R gradient was lost in both the *Prx1-Cre:Ptc1*$^{c/c}$ forelimb and hindlimb, with Gli3R levels being markedly reduced, particularly in the anterior (Fig. 2J). However, no clear increase in Gli3FL levels was observed in either limb.

Ptc1 inactivation in the hindlimb produces a molecular profile similar to that of *Gli3*$^{Xt/Xt}$

The effect of *Ptc1* inactivation on the expression of key limb patterning genes was investigated by whole-mount in situ hybridisation. In the hindlimb, changes in gene expression were most obvious at 11.5 dpc (Fig. 3A-L′). However, expression of *Fgf4*,

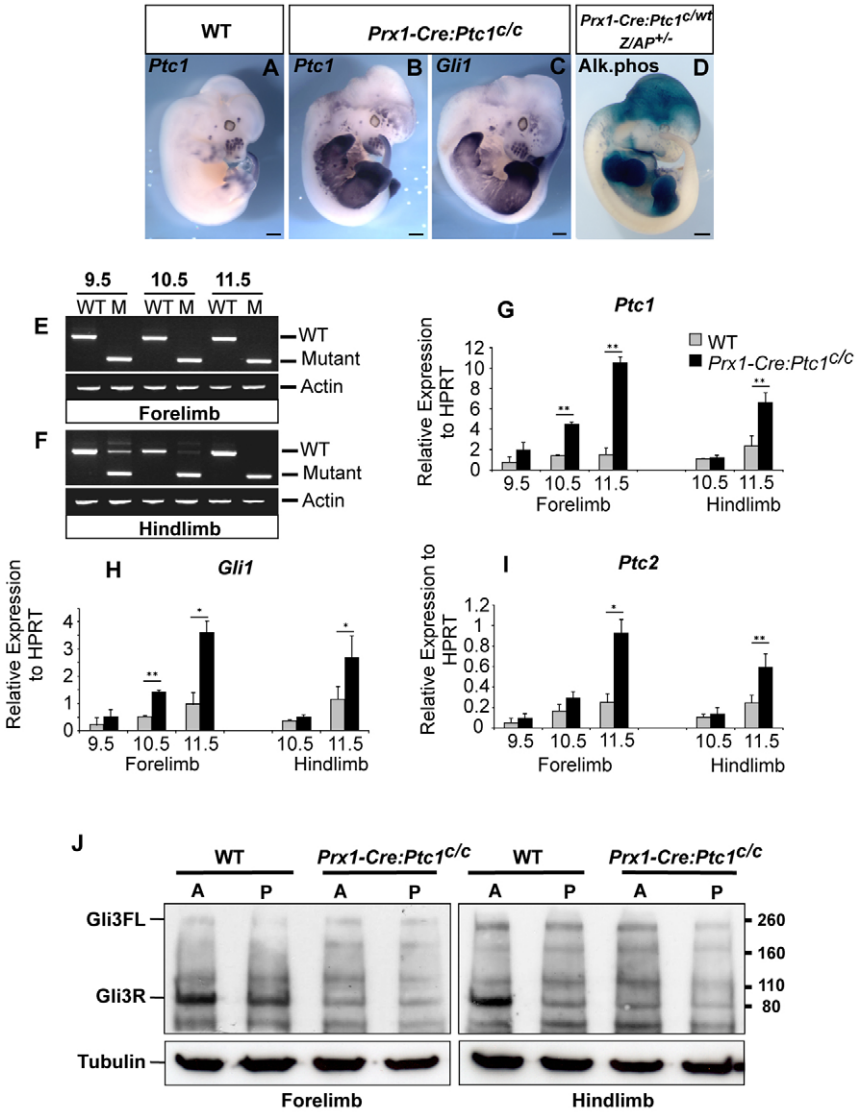

Fig. 2. Hh pathway upregulation at sites of *Prx1*-Cre activity. (**A-C**) Whole-mount wild-type and *Prx1-Cre:Ptc1*$^{c/c}$ embryos at 12.5 dpc, showing that *Ptc1* and *Gli1* upregulation in *Prx1-Cre:Ptc1*$^{c/c}$ embryos correlates closely with activity of *Prx1*-Cre (**D**), shown by alkaline phosphatase expression in a 12.0 dpc *Prx1-Cre:Ptc1*$^{c/wt}$*:Z/AP*$^{+/-}$ embryo (compare B and C with D). Scale bars: 500 μM. (**E**,**F**) RT-PCR of *Ptc1* exon 3 from wild-type (WT) and mutant (M) limbs detects only exon 3-deleted *Ptc1* at 9.5-11.5 dpc in the forelimb (E); the wild-type allele is still detectable in the hindlimb at 9.5-10.5 dpc, but not 11.5 dpc (F). Results are from representative samples of 9.5-11.5 dpc limbs, each consisting of two limbs. Due to variability in budding of the hindlimb at 9.5 dpc (21-29 somites), only one hindlimb pair was obtained from a 9.5 dpc embryo. For other stages, 2 (10.5 dpc), 3 (11.5 dpc) or 4 (9.5 dpc forelimb) samples were analysed. (**G-I**) Quantification of the delayed upregulation of *Ptc1*, *Gli1* and *Ptc2* in hindlimbs versus forelimbs (*P<0.05, **P<0.01). The single 9.5 dpc hindlimb sample was excluded from this analysis, and results from individual limb pairs were pooled for statistical analysis. (**J**) Western blot showing that Gli3R (83 kDa) is present in an AP gradient across the wild-type hindlimb, but is reduced in anterior *Prx1-Cre:Ptc1*$^{c/c}$ forelimbs and hindlimbs. No significant increase in levels of Gli3FL (190 kDa) is evident. α-tubulin (55 kDa) serves as a loading control.

Grem1, *Hand2*, *Hoxd13*, *Bmp2*, *Bmp4* and *Fgf8* was altered as early as 10.5 dpc (see Fig. S2A-G′ in the supplementary material). Additionally, at this stage ectopic *Ptc1* expression was weakly detectable in the anterior limb (Fig. S1B in the supplementary material), although the upregulation of *Ptc1* and *Gli1* detected by quantitative real-time PCR was not statistically significant at this point (Fig. 2G,H). From 11.5 dpc, *Prx1-Cre:Ptc1*$^{c/c}$ hindlimb buds displayed a small anterior domain of ectopic *Shh* expression, the hallmark of a group of polydactylous mouse mutants that includes *Gli3*$^{Xt/Xt}$ (Hill, 2007) (arrowhead, Fig. 3A′). The anterior mesenchyme of the *Prx1-Cre:Ptc1*$^{c/c}$ hindlimb also displayed expansion of *Grem1*, *Hand2*, *Hoxd11-Hoxd13* and *Jag1* at 11.5 dpc (Fig. 3B-E′; see also Fig. S2L-M′ in the supplementary material). Expression of the anteriorly restricted gene *Pax9* was abrogated in the mutant hindlimb, reflecting loss of Gli3R (Fig. 3F,F′), whereas the domain of *Gli3* expression appeared relatively unchanged although slightly expanded proximally (Fig. 3G,G′). In addition to gene expansion in the mesenchyme, the anterior AER of the *Prx1-Cre:Ptc1*$^{c/c}$ hindlimb displayed ectopic expression of *Bmp2*, *Bmp4*, *Fgf4* and *Fgf8* (Fig. 3H-K′). Consistent with this, the underlying mesenchyme ectopically expressed the downstream FGF target *Mkp3* (also known as *Dusp6*) (Kawakami et al., 2003), suggesting enhanced FGF signalling from the anterior AER (Fig. 3L,L′). In all cases, the anterior AER staining exhibited a sharp boundary, distinct from the anterior tapering normally revealed by *Fgf8* expression (Fig. 3K,K′, arrowhead). Discrete anterior expression of the above genes in the AER, together with *Shh* in the underlying mesenchyme, persisted in *Prx1-Cre:Ptc1*$^{c/c}$ hindlimbs until 12.5 dpc (or 13.5 dpc for *Fgf8*; Fig. 3M-Q′). Overall, the expression patterns of these genes correlate with their behaviour in the *Gli3*$^{Xt/Xt}$ limb (Bastida et al., 2004; Hill et al., 2007; Litingtung et al., 2002; McGlinn et al., 2005; te Welscher et al., 2002b), indicating that the two models are largely indistinguishable from one another during AP patterning stages.

Early *Ptc1* inactivation in the forelimb results in symmetrical expression of AP patterning genes

The molecular profile of the *Prx1-Cre:Ptc1*$^{c/c}$ forelimb was markedly different from that of the hindlimb. *Shh* expression was reduced and often lost from the ZPA (arrowheads, Fig. 4B and inset), and ectopic expression was redistributed along the distal anterior margin in 12 out of the 18 forelimbs analysed at 10.5 dpc (Fig. 4B), and in seven out of seven forelimbs analysed at 11.5 dpc (Fig. 4D). In the remaining six (out of 18) *Prx1-Cre:Ptc1*$^{c/c}$ forelimbs analysed at 10.5 dpc, *Shh* expression was completely undetectable (Fig. 4B, inset).

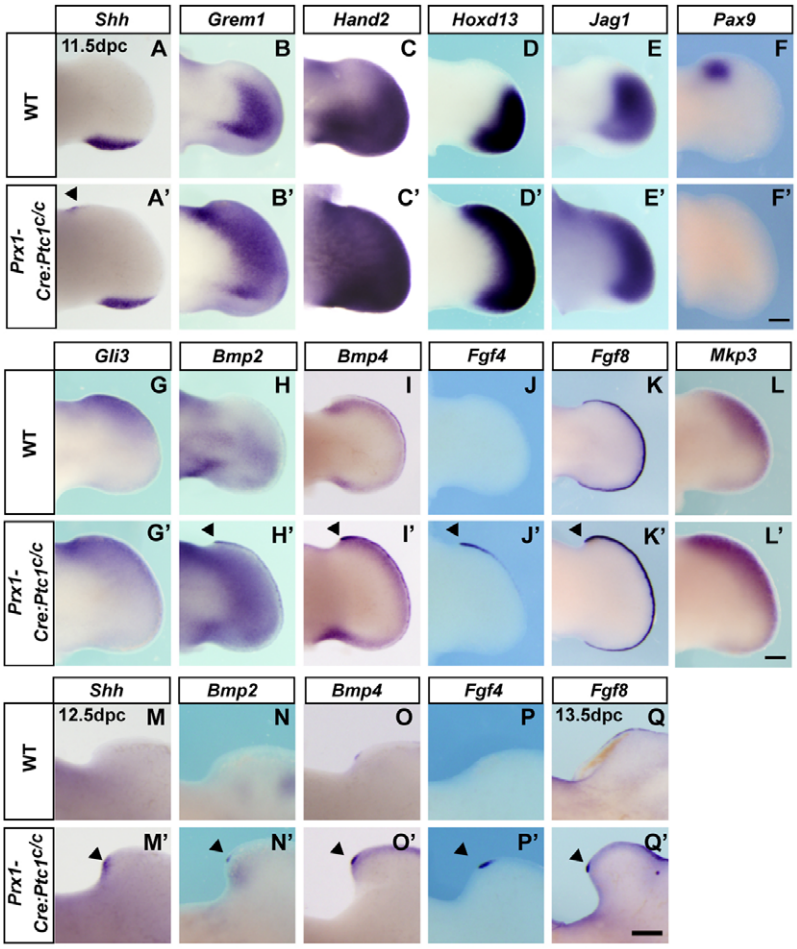

Fig. 3. Gene expression in *Prx1-Cre:Ptc1*$^{c/c}$ hindlimbs. Whole-mount in situ hybridisation of wild-type and *Prx1-Cre:Ptc1*$^{c/c}$ hindlimbs for the indicated genes. (**A-E′**) Expression of *Shh*, *Grem1*, *Hand2*, *Hoxd13*, and *Jag1* is expanded into the anterior 11.5 dpc *Prx1-Cre:Ptc1*$^{c/c}$ hindlimb. (**F-G′**) Expression of *Pax9* is abrogated in the *Prx1-Cre:Ptc1*$^{c/c}$ hindlimb (F,F′) and *Gli3* is relatively unchanged but slightly expanded proximally (G,G′). (**H-K′**) *Bmp2, Bmp4, Fgf4* and *Fgf8* are ectopically expressed in the anterior *Prx1-Cre:Ptc1*$^{c/c}$ hindlimb AER (arrowheads, H′-K′). (**L,L′**) *Mkp3* is expanded in the anterior mesenchyme of the *Prx1-Cre:Ptc1*$^{c/c}$ hindlimb at this stage. (**M-Q′**) The anterior AER region displays ectopic expression of *Shh* (underlying mesenchyme; M,M′, arrowhead), *Bmp2*, *Bmp4* and *Fgf4* at 12.5 dpc, and *Fgf8* at 13.5 dpc (N-Q′, arrowheads). Scale bars: 200 μM.

Although *Grem1* expression was detected in the anterior of most *Prx1-Cre:Ptc1*$^{c/c}$ forelimbs at 10.5-11.5 dpc, the size of the domain was reduced and showed a striking discontinuity (Fig. 4E-H; 4/8 at 10.5 dpc, 6/6 at 11.5 dpc). *Grem1* expression was undetectable in two out of eight mutant forelimbs, and its expression domain was equivalent in size to that seen in wild type in a further two limbs at 10.5 dpc (data not shown). In general, the proportion of 10.5 dpc forelimbs in which *Grem1* expression was reduced correlates loosely with the prevalent oligodactylous phenotype (75%). In accordance with the overall reduction in *Grem1* expression, *Fgf4* expression was not detected in the AER in 10 out of 14 forelimbs at 10.5 dpc (Fig. 4N), whereas in the remaining four limbs, *Fgf4* expression was shifted anteriorly to the central AER (Fig. 4N, inset). No *Fgf4* expression was observed from 11.5 dpc onwards in wild-type or *Prx1-Cre:Ptc1*$^{c/c}$ forelimbs (see Fig. S3J,J′ in the supplementary material).

Coupled with the loss of *Fgf4* from the AER in the majority of *Prx1-Cre:Ptc1*$^{c/c}$ forelimbs was a mild decrease in the length of the AER, as shown by *Fgf8* expression (Fig. 4I-L). A reduced domain of *Mkp3* expression was detected in the *Prx1-Cre:Ptc1*$^{c/c}$ forelimb at 10.5 dpc (Fig. 4O-P). Together with a similar reduction in other FGF targets, including *Spry1 and Spry4* (Minowada et al., 1999), at 10.5 dpc (Fig. S3E-F′ in the supplementary material), this suggests a decreased response to FGF signalling from the AER. Both *Mkp3* and *Grem1* expression were also downregulated at 9.75 dpc (Fig. 4Q-T), and overall these data support an early disruption of the Shh/Grem1/FGF loop in the mutant forelimb.

A striking phenomenon evident in the expression of virtually all of the genes examined in the *Prx1-Cre:Ptc1*$^{c/c}$ forelimb from 10.5 dpc was symmetry about the AP midline. Loss of *Pax9*, an anterior marker in the 11.5 dpc limb (McGlinn et al., 2005), suggests a loss of anterior identity (Fig. 5A,I). *Gli3* expression was reduced, although still visible in the anterior limb at 10.5 dpc (Fig. 5B,J), with remaining *Gli3* expression appearing symmetrical by 11.5 dpc (see Fig. S3K-K′ in the supplementary material). In addition, those genes normally restricted to the posterior limb were expressed in the anterior *Prx1-Cre:Ptc1*$^{c/c}$ forelimb (Fig. 5C-G,K-O). Expression of genes such as *Fgf4* (4/14; Fig. 4N, inset), *Hoxd11-Hoxd13* (Fig. 5C,K; see also Fig. S3M-O′ in the supplementary material) and *Hand2* (Fig. 5D,L), showed continuous expansion into the anterior. However, this was distinct from the expansion in the hindlimb as the expression domain was now symmetrical and, in the case of the Hoxd genes and *Fgf4*, was shifted centrally. Expression of *Bmp2* and *Bmp4* tended to occur as two distinct domains in the anterior and posterior mutant forelimb (Fig. 5F,G,N,O), which would suggest duplication of the posterior wild-type mesenchymal expression. This was further reinforced by the expression of the transcriptional repressor *Zfp503*, which we have previously shown to be downregulated in the anterior of both *Gli3*$^{Xt/Xt}$ and *Prx1-Cre:Ptc1*$^{c/c}$ hindlimbs (McGlinn et al., 2008; McGlinn et al., 2005). The distinct proximal domain of *Zfp503* expression visible at the autopod/zeugopod boundary of the posterior limb was duplicated in the anterior *Prx1-Cre:Ptc1*$^{c/c}$ forelimb, whereas the more distal anterior autopod expression was lost (Fig. 5H,P).

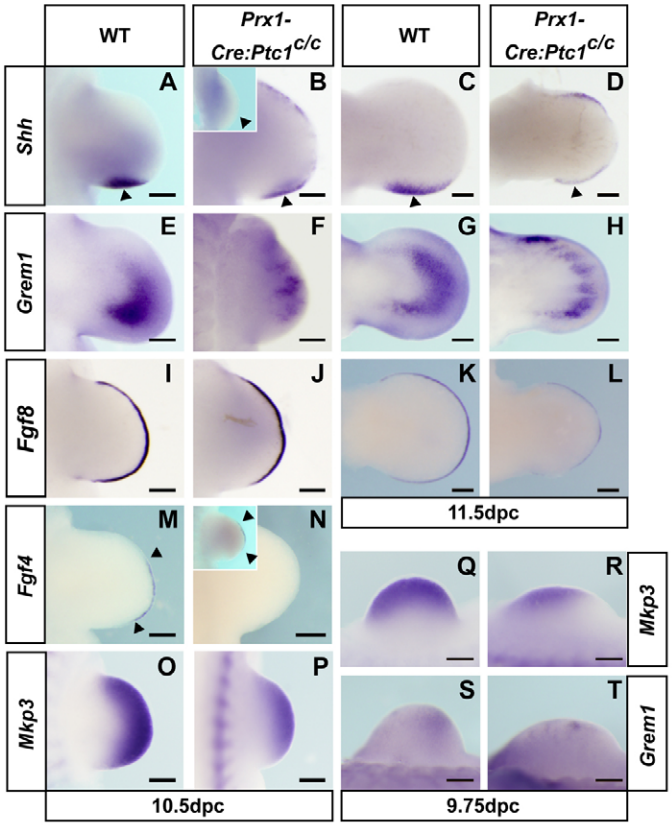

Fig. 4. ZPA/AER interactions are disrupted in *Prx1-Cre:Ptc1$^{c/c}$* forelimbs. Whole-mount in situ hybridisation of wild-type and *Prx1-Cre:Ptc1$^{c/c}$* forelimbs for the indicated genes. (**A-D**) At 10.5 dpc, *Shh* expression in *Prx1-Cre:Ptc1$^{c/c}$* forelimbs is redistributed from the ZPA (marked by arrowheads, A-D) to the anterior margin, with reduced (B) or completely undetectable (B, inset) ZPA expression; compare with wild type in A. At 11.5 dpc, *Shh* expression is reduced in the ZPA of *Prx1-Cre:Ptc1$^{c/c}$* forelimbs but is present in the anterior margin (D). (**E-H**) *Grem1* expression is anteriorly expanded in *Prx1-Cre:Ptc1$^{c/c}$* forelimbs but is reduced and discontinuous at 10.5 dpc (F) and 11.5 dpc (H). (**I-N**) The *Fgf8* expression domain is slightly shortened at 10.5 dpc (J) and 11.5 dpc (L) in *Prx1-Cre:Ptc1$^{c/c}$* forelimbs, and *Fgf4* expression is lost in most 10.5 dpc *Prx1-Cre:Ptc1$^{c/c}$* forelimbs (N), but is shifted centrally in a subset (approx. 28%) of limbs (N, inset). (**O-T**) *Mkp3* expression is reduced at 10.5 dpc (O-P), and *Mkp3* and *Grem1* are reduced at 9.75 dpc (27 somites; Q-T) in *Prx1-Cre:Ptc1$^{c/c}$* forelimbs. Scale bars: 200 μM.

Importantly, no such distinct anterior mesenchymal duplication of *Bmp2*, *Bmp4* or *Zfp503* expression was observed in the *Prx1-Cre:Ptc1$^{c/c}$* hindlimb (Fig. 3H′-I′) (see also McGlinn et al., 2008), which clearly demonstrates the dichotomy between the molecular profiles of the forelimb and hindlimb. Taken together, these data suggest that the anterior *Prx1-Cre:Ptc1$^{c/c}$* forelimb has undergone posterior re-specification.

To investigate pre-patterning and the generation of asymmetry in the forelimb, expression of *Hand2* was examined at 9.25 dpc (23 somites), prior to the establishment of the ZPA at around 9.5 dpc, and was found to be expanded into the anterior of the *Prx1-Cre:Ptc1$^{c/c}$* forelimb (Fig. 5Q,R). Mice ectopically expressing *Hoxd11-Hoxd13* across the forelimb bud displayed symmetrical limbs similar to the *Prx1-Cre:Ptc1$^{c/c}$* forelimb phenotype (Zakany et al., 2004). We therefore investigated 5′Hoxd gene expression in the early *Prx1-Cre:Ptc1$^{c/c}$* forelimb, prior to the onset of *Shh* expression. *Hoxd11* was ectopically expressed across the limb bud at 9.25 dpc (23 somites; Fig. 5S,T). Upregulation of *Hoxd13* in *Prx1-Cre:Ptc1$^{c/c}$* forelimbs was also observed at the 27 somite stage (data not shown). Thus, the precocious 5′Hoxd activity following the loss of *Ptc1* in the *Prx1-Cre:Ptc1$^{c/c}$* forelimb provides a likely mechanism for the symmetrical redistribution of *Shh*, *Hand2* and other patterning genes in these limbs.

We next sought to determine whether the changes in gene expression we observed in *Prx1-Cre:Ptc1$^{c/c}$* limbs were associated with a disruption in the apoptosis/proliferation balance. TUNEL analysis of 10.5 dpc limbs revealed no increase in apoptosis in *Prx1-Cre:Ptc1$^{c/c}$* limbs compared with that observed in wild type (Fig. 6A-D). This is consistent with a reduction in the *Msx1* and *Msx2* anterior expression domain at 10.5 and 11.5 dpc (see Fig. S3B-C′,H-I′ in the supplementary material), and suggests that neither Cre-mediated toxicity nor early apoptosis plays a major role in the forelimb phenotype. Some evidence of enhanced apoptosis in the central mesenchyme was detected at 12.5 dpc (data not shown), but as this later apoptosis occurs in both *Prx1:Ptc1$^{c/c}$* forelimbs and hindlimbs, it is unlikely to specifically affect early forelimb patterning events. At 11.5 dpc, a time when the size difference between mutant and wild-type limbs generally becomes obvious, proliferation levels were significantly increased in *Prx1-Cre:Ptc1$^{c/c}$* hindlimbs (P=0.001; Fig. 6E-H,I). Although a downward trend in proliferation was detected in the 11.5 dpc forelimb, no statistically significant change was observed (Fig. 6I). Hence neither altered apoptosis nor proliferation is likely to be the major determinant of the oligodactyly observed in *Prx1-Cre:Ptc1$^{c/c}$* forelimbs.

Prx1-Cre:Ptc1$^{c/c}$ limbs display reduced interdigital apoptosis and delayed AER regression

We next analysed the contribution of sustained Hh pathway activation to the relatively late process of digit separation, beyond the termination of Shh signalling in the wild-type limb. Results were identical for both limbs, and hindlimb data are presented here. Reduction of *Bmp2* and *Msx1* expression in the interdigital mesenchyme (IDM) of 12.5 dpc *Prx1-Cre:Ptc1$^{c/c}$* limbs (Fig. 6J-K,N-O) suggests that this tissue is not programmed to participate in the apoptotic pathway. Other BMP pathway members were also downregulated in the IDM at 12.5-13.5 dpc (see Fig. S4A-N′ in the supplementary material). Concomitantly, *Fgf8* expression persisted above the IDM of *Prx1-Cre:Ptc1$^{c/c}$* hindlimbs at 13.5 dpc, when the AER is regressing in wild-type limbs (Fig. 6L,P). TUNEL analysis also revealed that apoptosis of the IDM was markedly reduced in *Prx1-Cre:Ptc1$^{c/c}$* limbs relative to that observed in wild type (star, Fig. 6M,Q), even taking into account altered tissue integrity in some interdigital spaces. These data indicate that, in addition to early patterning changes, constitutive Hh signalling during digit morphogenesis inhibits the crucial process of apoptosis that is required for correct digit separation.

DISCUSSION

We have demonstrated for the first time the effects of unchecked ligand-independent upregulation of the Hh pathway specifically in the early limb mesenchyme by conditional ablation of functional *Ptc1*. Strikingly, we observe variable decrease or increase in digit number in the forelimb and hindlimb, respectively, together with posterior re-specification of the anterior forelimb. To our knowledge, this forelimb phenotype is unique amongst Hh gain-of-function mouse models, and we propose that this is primarily due to the timing and level of Hh pathway activation. Early inactivation of *Ptc1* in the *Prx1-Cre:Ptc1$^{c/c}$* forelimb reveals a key role for Hh

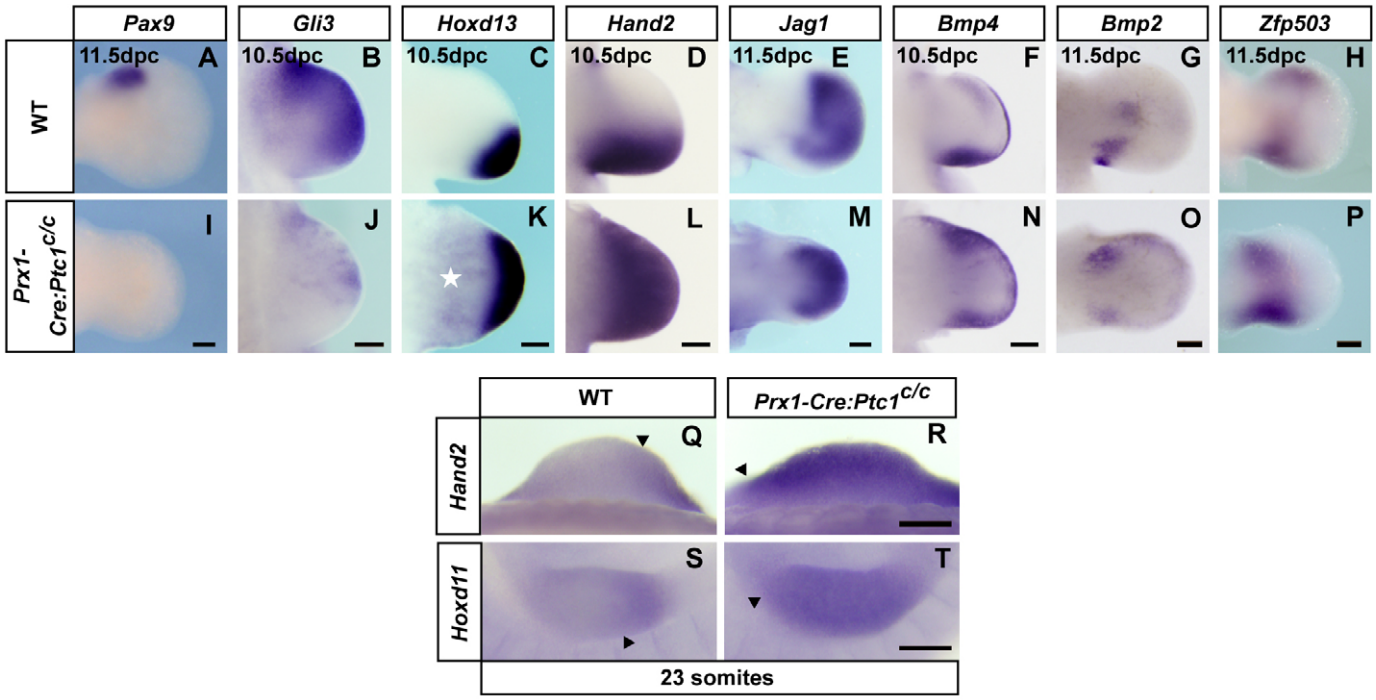

Fig. 5. Loss of asymmetry in *Prx1-Cre:Ptc1$^{c/c}$* forelimbs. (**A-T**) Whole-mount in situ hybridisation of wild-type and *Prx1-Cre:Ptc1$^{c/c}$* forelimbs for the indicated genes. *Pax9* (11.5 dpc) and *Gli3* (10.5 dpc) are anteriorly reduced in *Prx1-Cre:Ptc1$^{c/c}$* forelimbs (I,J) compared with in wild type (A,B). *Hoxd13* and *Hand2* are anteriorly expanded at 10.5 dpc in *Prx1-Cre:Ptc1$^{c/c}$* forelimbs (K,L) compared with in wild type (C,D). *Hoxd13* is also generally expanded in the more proximal mesenchyme in *Prx1-Cre:Ptc1$^{c/c}$* forelimbs (star, K). The posterior domains of *Jag1, Bmp4*, *Bmp2* and *Zfp503* are duplicated in the anterior *Prx1-Cre:Ptc1$^{c/c}$* forelimb (M-P; compare with wild type, E-H). *Hand2* and *Hoxd11* are anteriorly expanded in *Prx1-Cre:Ptc1$^{c/c}$* forelimbs at 9.25 dpc compared with in wild type (23 somites; Q-T). Scale bars: 200 μM.

pathway repression in early pre-patterning events prior to *Shh* expression in the ZPA, and results in perturbation of gene expression networks responsible for subsequent patterning (Fig. 7).

Ptc1 excision activates the Hh pathway

Prx1-Cre is expressed in limb mesenchyme as well as in restricted domains in other regions of the mouse embryo. Hh pathway activation in *Prx1-Cre:Ptc1$^{c/c}$* embryos, as determined by *Ptc1* and *Gli1* expression, was observed in domains that closely mirror sites of *Prx1*-Cre expression. This unexpected pathway activation outside the normal domains of detectable *Ptc1* expression is consistent with a model in which Hh signalling in these areas is normally inhibited by low-level *Ptc1* transcription, below the limits of in situ hybridisation detection. Upon removal of this functional *Ptc1* transcript, the pathway is activated inappropriately in a more widespread domain than anticipated. Our results, together with those from studies showing de-repression of *Ptc1-lacZ* expression in early *Ptc1* null embryos (Goodrich et al., 1997; Milenkovic et al., 1999), suggest that much of the embryonic mesenchyme is competent to respond to Hh signalling. This indicates that, in addition to maintaining the fine balance of signalling mediated by Hh ligands, negative regulation by Ptc1 in the absence of ligand is essential to maintain pathway repression in otherwise signalling-competent tissue. The finding that an expanded *Shh* domain is likely to underpin the drastic phenotype difference between the bat forelimb and hindlimb, suggests a precedent for evolutionary variation in the spatial restriction of Shh signalling as a means of controlling limb patterning to generate diversity (Hockman et al., 2008).

We determined the precise timing of *Ptc1* excision in *Prx1-Cre:Ptc1$^{c/c}$* limbs and found that, consistent with *Prx1*-Cre expression (Logan et al., 2002), there is a delay in excision in the hindlimb compared with in the forelimb, and this translates to a corresponding delay in pathway activation. The mutant hindlimb is therefore exposed to wild-type *Ptc1* transcript for a considerable time after the establishment of *Shh* expression. By contrast, *Ptc1* excision is virtually complete in most forelimbs prior to normal *Shh* expression, and this appears to lead to defects in the establishment of the ZPA. Our data and published results show that expression of *Prx1*-Cre throughout the forelimb mesenchyme at 9.5 dpc varies between individuals (Logan et al., 2002). Although this variability could explain the occurrence of polydactyly in a minority of forelimbs, we are not able to confirm this with our model.

Early expression cascades are perturbed in the symmetrical *Prx1-Cre:Ptc1$^{c/c}$* forelimb

In contrast to the asymmetry in *Prx1-Cre:Ptc1$^{c/c}$* hindlimbs, mutant forelimbs appear largely morphologically and molecularly symmetrical about the midline (Fig. 7B). Although embryonic lethality prevents unequivocal determination of digit identity in the *Prx1-Cre:Ptc1$^{c/c}$* forelimbs, anterior expansion of *Hoxd11* and *Hoxd12* implies that digit 1 identity is lost, as *Hoxd11* and *Hoxd12* expression in the wild-type limb is excluded from the digit 1 primordium (Kmita et al., 2005; Nelson et al., 1996). Importantly, this distinguishes the oligodactyly of the *Prx1-Cre:Ptc1$^{c/c}$* forelimb from that produced by *Shh* inactivation, in which digit 1 identity is preserved in the absence of all other digits (Chiang et al., 2001). The lack of extensive ectopic anterior cell death at 10.5 dpc, as seen in

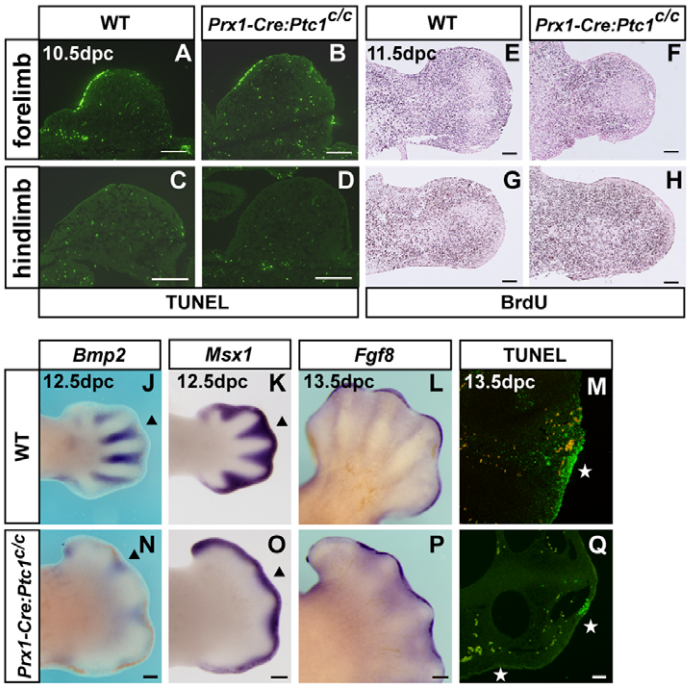

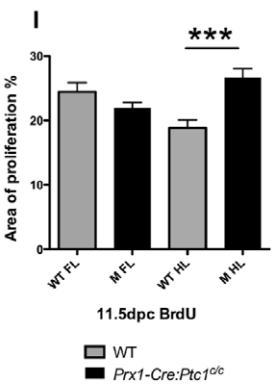

Fig. 6. Apoptosis and proliferation in *Prx1-Cre:Ptc1*$^{c/c}$ limbs. (**A-D**) Apoptosis is unchanged in 10.5 dpc *Prx1-Cre:Ptc1*$^{c/c}$ limbs from that in wild type, as assessed by TUNEL. (**E-I**) At 11.5 dpc, proliferation measured by BrdU incorporation was significantly increased in *Prx1-Cre:Ptc1*$^{c/c}$ hindlimbs but not forelimbs (***P=0.001). (**J-K**,**N-O**) Expression of *Bmp2* and *Msx1* is reduced in the IDM at 12.5 dpc in *Prx1-Cre:Ptc1*$^{c/c}$ limbs compared with in wild type. (**L**,**P**) At 13.5 dpc, *Fgf8* persists above the interdigits in *Prx1-Cre:Ptc1*$^{c/c}$ limbs. (**M**,**Q**) The IDM of sectioned 13.5 dpc *Prx1-Cre:Ptc1*$^{c/c}$ limbs contains fewer apoptotic cells than wild type, as assessed by TUNEL (stars). Scale bars: 500 μM in Q; 200 μM in all other panels.

the posteriorised limbs of *Msx1/2* mouse mutants (Lallemand et al., 2005), indicates that the symmetrical *Prx1-Cre:Ptc1*$^{c/c}$ forelimb phenotype is unlikely to reflect a loss of anterior tissue. This, and the expression of normally posteriorly restricted genes in the anterior limb, suggest that the symmetrical forelimb results from re-specification of anterior tissue to a posterior identity.

Limb asymmetry and establishment of the ZPA is determined by interplay between 5′Hoxd genes, *Gli3* and *Hand2* in the early limb bud (Tarchini et al., 2006; te Welscher et al., 2002a; Zakany et al., 2004). Our data show that early inactivation of *Ptc1* in the forelimb disturbs these early patterning events, as judged by the anterior expansion of *Hoxd11* and *Hand2* expression at 9.25 dpc (23 somites), and of *Hoxd13* slightly later (27 somites). By contrast, there is no change in expression of these genes between wild-type and *Prx1-Cre:Ptc1*$^{c/c}$ hindlimbs at the equivalent stage. In a previous study, inactivation of *Shh* using *Prx1*-Cre produced a hypomorphic phenotype (Lewis et al., 2001), suggesting that this driver does not inactivate gene expression in all cells prior to *Shh* expression. Indeed, it is likely that a small fraction of cells escape *Ptc1* excision prior to the normal onset of *Shh* pathway activation in the *Prx1-Cre:Ptc1*$^{c/c}$ forelimb. However, our data indicate that a high enough level of *Ptc1* inactivation is achieved to drive downstream signalling to a sufficient threshold to perturb pre-patterning.

Following early expansion of *Hoxd11* and *Hand2* expression across the entire *Prx1-Cre:Ptc1*$^{c/c}$ forelimb paddle, *Shh* expressing cells are visible around the distal limb periphery. Similar changes in *Shh* expression are induced by ectopic anterior expression of *Hand2* (McFadden et al., 2002), and 5′Hoxd genes (Zakany et al., 2004). In these cases, limbs show a loss of asymmetry and a conversion of anterior digits to posterior identities (McFadden et al., 2002; Zakany et al., 2004). The ectopic *Hoxd11-Hoxd13* expression in the latter model also produces variable oligodactyly (Zakany et al., 2004), which further implicates early ectopic 5′Hoxd gene expression in the generation of the *Prx1-Cre:Ptc1*$^{c/c}$ forelimb phenotype. Although the limb symmetry in these other mouse models is likely to be caused by the distally expanded *Shh*, this is unlikely to be a major contributing factor in the *Prx1-Cre:Ptc1*$^{c/c}$ forelimb phenotype, because this limb is characterised by widespread high-level ectopic Hh pathway activation. It is more likely that signalling events downstream of the constitutively active Hh pathway underpin the forelimb symmetry, although a contribution of properties intrinsic to the redistributed *Shh*-expressing cells and their descendants cannot be ruled out.

The Shh/Grem1/FGF signalling loop is disrupted in *Prx1-Cre:Ptc1*$^{c/c}$ forelimbs

To date, activation of Hh signalling in both mouse models and human dysmorphologies has generally been associated with extra digits (Hill et al., 2003). Although we observe this phenotype in the *Prx1-Cre:Ptc1*$^{c/c}$ hindlimbs, the forelimbs predominantly display an oligodactylous phenotype with an average of 3-4 digits. Analysis of Gli3 processing at 11.5 dpc revealed that the Gli3FL:Gli3R gradient is abolished in both forelimbs and hindlimbs in a similar manner. In both cases there is a decrease in Gli3R levels in the anterior limb, consistent with inhibition of Gli3 cleavage by Shh signalling (Wang et al., 2000), although a clear increase in Gli3FL was not detectable by western blotting. These data suggest that the forelimb-specific phenotype is not due to differences in Gli3 cleavage.

Early reduced expression of *Mkp3* and other targets of AER-FGF signalling suggests that the mesenchymal response to FGF signalling is attenuated specifically in the *Prx1-Cre:Ptc1*$^{c/c}$ forelimb. This reduced response corresponds to a lack of *Fgf4* expression in most limbs, and to a relatively subtle shortening of the *Fgf8* expression domain. However, mice lacking *Fgf4* do not display limb defects (Moon et al., 2000; Sun et al., 2000), and recent studies demonstrate conclusively that of all the AER FGFs, *Fgf8* is sufficient for limb patterning (Mariani et al., 2008). Thus, the reduction in *Fgf4* expression is unlikely to be the major cause of the *Prx1-Cre:Ptc1*$^{c/c}$ forelimb phenotype, but it is nevertheless indicative of perturbation of the Shh/Grem1/FGF loop (Verheyden and Sun, 2008). Accordingly, we detected evidence of reduced *Grem1* expression in the *Prx1-Cre:Ptc1*$^{c/c}$ forelimb very early after limb budding. Although Shh normally maintains expression of *Grem1* in the limb, *Shh*-expressing

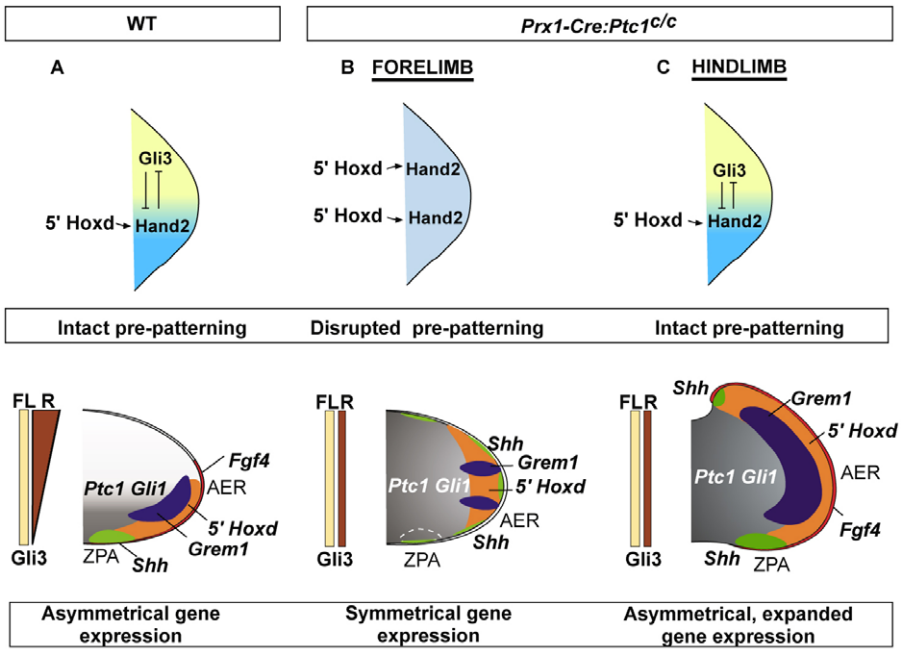

Fig. 7. A summary of the gene expression changes in *Prx1-Cre:Ptc1$^{c/c}$* limbs. Interplay between 5′Hoxd genes, *Gli3* and *Hand2* establishes limb asymmetry in wild-type (WT) limbs primarily by determining correct formation of the posterior *Shh*-expressing ZPA (**A**). Constitutive Hh signalling in *Prx1-Cre:Ptc1$^{c/c}$* limbs occurs prior to (forelimb, **B**) and subsequent to (hindlimb, **C**) early patterning. Early and strong Hh signalling in *Prx1-Cre:Ptc1$^{c/c}$* forelimbs disrupts the pre-pattern and generates mirror-image symmetry of gene expression (B). Pre-patterning is intact in *Prx1-Cre:Ptc1$^{c/c}$* hindlimbs, which predominantly display anterior expansion of genes (C).

cells and their descendants cannot express *Grem1*, a fact attributed to very high levels of autocrine Shh signalling (Nissim et al., 2006; Scherz et al., 2004). Early high-level autocrine activation of the Hh pathway across the *Prx1-Cre;Ptc1$^{c/c}$* forelimb might therefore mediate an early reduced capacity for cells to express *Grem1*, thus disturbing the Shh/Grem1/FGF loop. We favour this over a more direct effect on the later FGF/Grem1 inhibitory loop (Verheyden and Sun, 2008), as the early reduced expression domain of *Mkp3* at 9.75 dpc is inconsistent with the high levels of FGF signalling required to repress *Grem1*. Given that a primary feature of the *Prx1-Cre:Ptc1$^{c/c}$* forelimb is the widespread upregulation of 5′Hoxd genes, it may be that high-level constitutive Hh pathway activity is acting through this early ectopic Hox gene expression to downregulate *Grem1*. This leads to the intriguing but speculative hypothesis that high levels of 5′Hoxd genes contribute to the refractoriness to *Grem1* expression in *Shh* lineage cells of the wild-type limb.

Like the *Prx1-Cre:Ptc1$^{c/c}$* forelimb, *Grem1* null limbs are characterised by fewer digits, but they also display reduced Shh signalling and increased apoptosis (Khokha et al., 2003; Michos et al., 2004). By contrast, we see no evidence of enhanced early forelimb-specific apoptosis in the *Prx1-Cre;Ptc1$^{c/c}$* model. Furthermore, we demonstrate a reduction in the anterior expression domain of *Msx1* and *Msx2,* which are thought to mediate apoptosis downstream of both Shh/Gli3R and BMP signalling in the limb (Lallemand et al., 2009; Pizette et al., 2001). Although reduced Msx gene expression is not consistent with the observed expanded anterior expression of *Bmp2* and *Bmp4*, it supports a recent suggestion that anterior Msx gene expression might be mediated predominantly by Gli3R (Lallemand et al., 2009). This is further supported by the selective maintenance of Msx gene expression in the most anterior region of the limbs of *Bmpr1a* conditional-knockout mice (Ovchinnikov et al., 2006). Conversely, despite the duplication of both *Bmp2* and *Bmp4* expression domains, a decrease in overall BMP signalling in the *Prx1-Cre:Ptc1$^{c/c}$* forelimb cannot be ruled out. However, this is less likely in those limbs lacking *Fgf4,* as it has been shown that inhibition of BMP signalling allows FGF expression in the AER (Capdevila et al., 1999; Pizette and Niswander, 1999; Zuniga et al., 1999).

While much effort has focused on the mechanisms underlying the positive potentiation of the posteriorly biased expression of *Shh*, our data highlight a previously unappreciated requirement for Ptc1-mediated negative control over the precise timing and levels of Shh signalling in the developing limb. Importantly, the *Prx1-Cre:Ptc1$^{c/c}$* forelimb phenotype suggests that failure to prevent activation of this pathway throughout the early pre-patterning stages of limb budding results in perturbations to key gene expression cascades responsible for defining limb asymmetry and digit number.

Acknowledgements

We thank C. Tabin, P. Koopman, M. Little and D. Ovchinnikov for kindly providing probes with permission from cited sources, M. Logan for the *Prx1-Cre* mouse line, and B. Wang for the Gli3 antibody. We also thank C. C. Hui, R. Villani and T. Ellis for helpful discussion, and A. Hardacre, J. Conway and T. Davidson for assistance with mouse husbandry. This work was supported by the National Health and Medical Research Council of Australia (NHMRC). N.C.B. was a recipient of an Australian Postgraduate Award, and C.W. is an NHMRC Senior Research Fellow.

Supplementary material

Supplementary material for this article is available at
http://dev.biologists.org/cgi/content/full/136/20/3515/DC1

References

Bastida, M. F., Delgado, M. D., Wang, B., Fallon, J. F., Fernandez-Teran, M. and Ros, M. A. (2004). Levels of Gli3 repressor correlate with Bmp4 expression and apoptosis during limb development. *Dev. Dyn.* **231**, 148-160.

Benazet, J. D., Bischofberger, M., Tiecke, E., Goncalves, A., Martin, J. F., Zuniga, A., Naef, F. and Zeller, R. (2009). A self-regulatory system of interlinked signaling feedback loops controls mouse limb patterning. *Science* **323**, 1050-1053.

Bruce, S. J., Gardiner, B. B., Burke, L. J., Gongora, M. M., Grimmond, S. M. and Perkins, A. C. (2007). Dynamic transcription programs during ES cell differentiation towards mesoderm in serum versus serum-freeBMP4 culture. *BMC Genomics* **8**, 365.

Capdevila, J., Tsukui, T., Rodriquez Esteban, C., Zappavigna, V. and Izpisua Belmonte, J. C. (1999). Control of vertebrate limb outgrowth by the proximal factor Meis2 and distal antagonism of BMPs by Gremlin. *Mol. Cell* **4**, 839-849.

Chen, W., John, J., Lin, C. and Chang, C. (2002). Molecular cloning and developmental expression of zinc finger transcription factor MTF-1 gene in zebrafish, Danio rerio. *Biochem. Biophys. Res. Commun.* **291**, 798-805.

Chen, Y. and Struhl, G. (1996). Dual roles for patched in sequestering and transducing Hedgehog. *Cell* **87**, 553-563.

Chen, Y., Knezevic, V., Ervin, V., Hutson, R., Ward, Y. and Mackem, S. (2004). Direct interaction with Hoxd proteins reverses Gli3-repressor function to promote digit formation downstream of Shh. *Development* **131**, 2339-2347.
Chiang, C., Litingtung, Y., Harris, M. P., Simandl, B. K., Li, Y., Beachy, P. A. and Fallon, J. F. (2001). Manifestation of the limb prepattern: limb development in the absence of sonic hedgehog function. *Dev. Biol.* **236**, 421-435.
Ellis, T., Smythe, I., Riley, E., Graham, S., Elliot, K., Narang, M., Kay, G., Wicking, C. and Wainwright, B. (2003). Patched1 conditional null allele in mice. *Genesis* **36**, 158-161.
Fowles, L. F., Bennetts, J. S., Berkman, J. L., Williams, E., Koopman, P., Teasdale, R. D. and Wicking, C. (2003). Genomic screen for genes involved in mammalian craniofacial development. *Genesis* **35**, 73-87.
Goodrich, L. V., Johnson, R. L., Milenkovic, L., McMahon, J. A. and Scott, M. P. (1996). Conservation of the hedgehog/patched signaling pathway from flies to mice: induction of a mouse patched gene by Hedgehog. *Genes Dev.* **10**, 301-312.
Goodrich, L. V., Milenkovic, L., Higgins, K. M. and Scott, M. P. (1997). Altered neural cell fates and medulloblastoma in mouse patched mutants. *Science* **277**, 1109-1113.
Hahn, H., Christiansen, J., Wicking, C., Zaphiropoulos, P. G., Chidambaram, A., Gerrard, B., Vorechovsky, I., Bale, A. E., Toftgard, R., Dean, M. et al. (1996). A mammalian patched homolog is expressed in target tissues of sonic hedgehog and maps to a region associated with developmental abnormalities. *J. Biol. Chem.* **271**, 12125-12128.
Hill, P., Wang, B. and Ruther, U. (2007). The molecular basis of Pallister-Hall associated polydactyly. *Hum. Mol. Genet.* **16**, 2089-2096.
Hill, P., Gotz, K. and Ruther, U. (2009). A SHH-independent regulation of Gli3 is a significant determinant of anteroposterior patterning of the limb bud. *Dev. Biol.* **328**, 506-516.
Hill, R. E. (2007). How to make a zone of polarizing activity: insights into limb development via the abnormality preaxial polydactyly. *Dev. Growth Differ.* **49**, 439-448.
Hill, R. E., Heaney, S. J. and Lettice, L. A. (2003). Sonic hedgehog: restricted expression and limb dysmorphologies. *J. Anat.* **202**, 13-20.
Hockman, D., Cretekos, C. J., Mason, M. K., Behringer, R. R., Jacobs, D. S. and Illing, N. (2008). A second wave of Sonic hedgehog expression during the development of the bat limb. *Proc. Natl. Acad. Sci. USA* **105**, 16982-16987.
Hui, C. C. and Joyner, A. L. (1993). A mouse model of greig cephalopolysyndactyly syndrome: the extra-toes^{J} mutation contains an intragenic deletion of the Gli3 gene. *Nat. Genet.* **3**, 241-246.
Ingham, P. W. and McMahon, A. P. (2001). Hedgehog signaling in animal development: paradigms and principles. *Genes Dev.* **15**, 3059-3087.
Kawakami, Y., Rodriguez-Leon, J., Koth, C. M., Buscher, D., Itoh, T., Raya, A., Ng, J. K., Esteban, C. R., Takahashi, S., Henrique, D. et al. (2003). MKP3 mediates the cellular response to FGF8 signalling in the vertebrate limb. *Nat. Cell Biol.* **5**, 513-519.
Khokha, M. K., Hsu, D., Brunet, L. J., Dionne, M. S. and Harland, R. M. (2003). Gremlin is the BMP antagonist required for maintenance of Shh and Fgf signals during limb patterning. *Nat. Genet.* **34**, 303-307.
Kmita, M., Tarchini, B., Zakany, J., Logan, M., Tabin, C. J. and Duboule, D. (2005). Early developmental arrest of mammalian limbs lacking HoxA/HoxD gene function. *Nature* **435**, 1113-1116.
Lallemand, Y., Nicola, M. A., Ramos, C., Bach, A., Cloment, C. S. and Robert, B. (2005). Analysis of Msx1; Msx2 double mutants reveals multiple roles for Msx genes in limb development. *Development* **132**, 3003-3014.
Lallemand, Y., Bensoussan, V., Cloment, C. S. and Robert, B. (2009). Msx genes are important apoptosis effectors downstream of the Shh/Gli3 pathway in the limb. *Dev. Biol.* **331**, 189-198.
Lewis, P. M., Dunn, M. P., McMahon, J. A., Logan, M., Martin, J. F., St-Jacques, B. and McMahon, A. P. (2001). Cholesterol modification of sonic hedgehog is required for long-range signaling activity and effective modulation of signaling by Ptc1. *Cell* **105**, 599-612.
Litingtung, Y., Dahn, R. D., Li, Y., Fallon, J. F. and Chiang, C. (2002). Shh and Gli3 are dispensable for limb skeleton formation but regulate digit number and identity. *Nature* **418**, 979-983.
Lobe, C. G., Koop, K. E., Kreppner, W., Lomeli, H., Gertsenstein, M. and Nagy, A. (1999). Z/AP, a double reporter for cre-mediated recombination. *Dev. Biol.* **208**, 281-292.
Logan, M., Martin, J., Nagy, A., Lobe, C., Olson, E. N. and Tabin, C. (2002). Expression of Cre recombinase in the developing mouse limb bud driven by a Prx1 enhancer. *Genesis* **33**, 77-80.
Mariani, F. V., Ahn, C. P. and Martin, G. R. (2008). Genetic evidence that FGFs have an instructive role in limb proximal-distal patterning. *Nature* **453**, 401-405.
Marigo, V., Davey, R. A., Zuo, Y., Cunningham, J. M. and Tabin, C. J. (1996a). Biochemical evidence that patched is the Hedgehog receptor. *Nature* **384**, 176-179.
Marigo, V., Johnson, R. L., Vortkamp, A. and Tabin, C. J. (1996b). Sonic hedgehog differentially regulates expression of GLI and GLI3 during limb development. *Dev. Biol.* **180**, 273-283.
McFadden, D. G., McAnally, J., Richardson, J. A., Charite, J. and Olson, E. N. (2002). Misexpression of dHAND induces ectopic digits in the developing limb bud in the absence of direct DNA binding. *Development* **129**, 3077-3088.
McGlinn, E. and Tabin, C. J. (2006). Mechanistic insight into how Shh patterns the vertebrate limb. *Curr. Opin. Genet. Dev.* **16**, 426-432.
McGlinn, E., van Bueren, K. L., Fiorenza, S., Mo, R., Poh, A. M., Forrest, A., Soares, M. B., Bonaldo Mde, F., Grimmond, S., Hui, C. C. et al. (2005). Pax9 and Jagged1 act downstream of Gli3 in vertebrate limb development. *Mech. Dev.* **122**, 1218-1233.
McGlinn, E., Richman, J. M., Metzis, V., Town, L., Butterfield, N. C., Wainwright, B. J. and Wicking, C. (2008). Expression of the NET family member Zfp503 is regulated by hedgehog and BMP signaling in the limb. *Dev. Dyn.* **237**, 1172-1182.
Michos, O., Panman, L., Vintersten, K., Beier, K., Zeller, R. and Zuniga, A. (2004). Gremlin-mediated BMP antagonism induces the epithelial-mesenchymal feedback signaling controlling metanephric kidney and limb organogenesis. *Development* **131**, 3401-3410.
Milenkovic, L., Goodrich, L. V., Higgins, K. M. and Scott, M. P. (1999). Mouse patched1 controls body size determination and limb patterning. *Development* **126**, 4431-4440.
Minowada, G., Jarvis, L. A., Chi, C. L., Neubuser, A., Sun, X., Hacohen, N., Krasnow, M. A. and Martin, G. R. (1999). Vertebrate Sprouty genes are induced by FGF signaling and can cause chondrodysplasia when overexpressed. *Development* **126**, 4465-4475.
Moon, A. M., Boulet, A. M. and Capecchi, M. R. (2000). Normal limb development in conditional mutants of Fgf4. *Development* **127**, 989-996.
Nelson, C. E., Morgan, B. A., Burke, A. C., Laufer, E., DiMambro, E., Murtaugh, L. C., Gonzales, E., Tessarollo, L., Parada, L. F. and Tabin, C. (1996). Analysis of Hox gene expression in the chick limb bud. *Development* **122**, 1449-1466.
Nissim, S., Hasso, S. M., Fallon, J. F. and Tabin, C. J. (2006). Regulation of Gremlin expression in the posterior limb bud. *Dev. Biol.* **299**, 12-21.
Ovchinnikov, D. A., Selever, J., Wang, Y., Chen, Y. T., Mishina, Y., Martin, J. F. and Behringer, R. R. (2006). BMP receptor type IA in limb bud mesenchyme regulates distal outgrowth and patterning. *Dev. Biol.* **295**, 103-115.
Pizette, S. and Niswander, L. (1999). BMPs negatively regulate structure and function of the limb apical ectodermal ridge. *Development* **126**, 883-894.
Pizette, S., Abate-Shen, C. and Niswander, L. (2001). BMP controls proximodistal outgrowth, via induction of the apical ectodermal ridge, and dorsoventral patterning in the vertebrate limb. *Development* **128**, 4463-4474.
Riddle, R. D., Johnson, R. L., Laufer, E. and Tabin, C. (1993). Sonic hedgehog mediates the polarizing activity of the ZPA. *Cell* **75**, 1401-1416.
Roelink, H., Augsburger, A., Heemskerk, J., Korzh, V., Norlin, S., Ruiz i Altaba, A., Tanabe, Y., Placzek, M., Edlund, T., Jessell, T. M. et al. (1994). Floor plate and motor neuron induction by vhh-1, a vertebrate homolog of hedgehog expressed by the notochord. *Cell* **76**, 761-775.
Scherz, P. J., Harfe, B. D., McMahon, A. P. and Tabin, C. J. (2004). The limb bud Shh-Fgf feedback loop is terminated by expansion of former ZPA cells. *Science* **305**, 396-399.
Sun, X., Lewandoski, M., Meyers, E. N., Liu, Y. H., Maxson, R. E., Jr and Martin, G. R. (2000). Conditional inactivation of Fgf4 reveals complexity of signalling during limb bud development. *Nat. Genet.* **25**, 83-86.
Tarchini, B., Duboule, D. and Kmita, M. (2006). Regulatory constraints in the evolution of the tetrapod limb anterior-posterior polarity. *Nature* **443**, 985-988.
te Welscher, P., Fernandez-Teran, M., Ros, M. A. and Zeller, R. (2002a). Mutual genetic antagonism involving GLI3 and dHAND prepatterns the vertebrate limb bud mesenchyme prior to SHH signaling. *Genes Dev.* **16**, 421-426.
te Welscher, P., Zuniga, A., Kuijper, S., Drenth, T., Goedemans, H. J., Meijlink, F. and Zeller, R. (2002b). Progression of vertebrate limb development through SHH-mediated counteraction of GLI3. *Science* **298**, 827-830.
Verheyden, J. M. and Sun, X. (2008). An Fgf/Gremlin inhibitory feedback loop triggers termination of limb bud outgrowth. *Nature* **454**, 638-641.
Wang, B., Fallon, J. F. and Beachy, P. A. (2000). Hedgehog-regulated processing of Gli3 produces an anterior/posterior repressor gradient in the developing vertebrate limb. *Cell* **100**, 423-434.
Wang, C., Pan, Y. and Wang, B. (2007a). A hypermorphic mouse Gli3 allele results in a polydactylous limb phenotype. *Dev. Dyn.* **236**, 769-776.
Wang, C., Ruther, U. and Wang, B. (2007b). The Shh-independent activator function of the full-length Gli3 protein and its role in vertebrate limb digit patterning. *Dev. Biol.* **305**, 460-469.
Zakany, J., Kmita, M. and Duboule, D. (2004). A dual role for Hox genes in limb anterior-posterior asymmetry. *Science* **304**, 1669-1672.
Zuniga, A., Haramis, A. P., McMahon, A. P. and Zeller, R. (1999). Signal relay by BMP antagonism controls the SHH/FGF4 feedback loop in vertebrate limb buds. *Nature* **401**, 598-602.